



#### Available online at www.sciencedirect.com

# **ScienceDirect**

Geochimica et Cosmochimica Acta 255 (2019) 237-246

## Geochimica et Cosmochimica Acta

www.elsevier.com/locate/gca

# Hydrothermal oxidation of Os

## Dionysis I. Foustoukos

Geophysical Laboratory, Carnegie Institution of Washington, 5251 Broad Branch Rd. NW, Washington, DC 20015, United States

Received 7 November 2018; accepted in revised form 19 April 2019; available online 26 April 2019

#### Abstract

A series of hydrothermal diamond anvil cell experiments was conducted to investigate the mobility of Os and Ir in saline and oxidizing hydrothermal fluids as function of fluid pH at temperatures ranging from 500 °C to 1000 °C and pressures resembling upper mantle/lower crust environments (29–1343 MPa). The composition of reactant fluids was monitored in real time and at in situ conditions by Raman vibrational spectroscopy. Results revealed the formation of Os=O volatile aqueous species under oxidizing redox conditions ( $\sim$ +5  $\Delta$ FMQ) and at temperatures exceeding 850 °C. These species were detected in an immiscible phase separated from the homogeneous fluid at low pressure conditions (<150 MPa). Based on previous experimental and theoretical studies, the Os-bearing species observed in situ are attributed to the presence of OsO<sub>4(g)</sub>. Volatile transport of Os in high temperature/pressure magmatic fluids, therefore, may include oxide aqueous species along with Os-Cl complexation. Possible evidence of Ir oxidation was provided by the formation of H<sub>2(aq)</sub> in Ir-H<sub>2</sub>O experiments at 700–800 °C and pressures of 543–793 MPa. Experimental data support the role of slab-derived fluids in yielding elevated Os/Ir ratios in metasomatized xenoliths relative to primitive upper mantle composition through the enhanced mobility of Os in the form of Cl- and oxygen-bearing volatile aqueous complexes. © 2019 Elsevier Ltd. All rights reserved.

Keywords: Supercritical fluids; Brines; Os; OsO<sub>4</sub>; Ir; Hydrothermal diamond anvil cell; Raman vibrational spectroscopy; Mantle metasomatism; Os isotope systematics

## 1. INTRODUCTION

Crustal fluids circulating within the subducting slab and the mantle wedge are considered to be alkaline (pH < 8, 25 °C), saline and enriched in C—O—H volatiles (e.g. CO<sub>2</sub>, H<sub>2</sub>) under conditions reflecting dehydration and decarbonation of the subducted oceanic lithosphere (Frezzotti and Ferrando, 2015; Keppler, 2017). The slab-derived fluids are introduced in island are volcanoes and infiltrate the sub-arc mantle resulting in the metasomatism of mantle xenoliths (Carlson, 2005; Alard et al., 2011). The extent and conditions of metasomatic processes imposed on ultramafic lithologies associated with the arc settings is often constrained by the distribution of highly siderophile elements such as Os, Re, Ir and Pt, Pd and Ru with a particular emphasis on the Re-Os isotope systematics.

E-mail address: dfoustoukos@ciw.edu

For example, xenoliths that have been altered by slabderived fluids appear to be enriched in Os relative to Ir while maintaining radiogenic <sup>187</sup>Os/<sup>188</sup>Os compositions indicative of contributions from sources with high time-(McInnes et al., 1999; averaged Re/Os ratios Kepezhinskas et al., 2002; Lee, 2002; Alard et al., 2011; Rielli et al., 2018). Infiltration of slab-derived fluids has also been associated with the scavenging of mantle Os resulting in its depletion relative to the other highly siderophile elements (Brandon et al., 1996; Widom et al., 2003; Saha et al., 2005; Senda et al., 2007; Suzuki et al., 2011; Widom, 2011; Liu et al., 2018). In all cases, the apparent Os mobility has been attributed to the interaction of xenoliths with saline and oxidizing fluids that promote Os dissolution through the development of chloro complexes (Wood, 1987; Xiong and Wood, 2000). Furthermore, elevated concentrations of Os in gas condensates from volcanic emissions have been linked to elemental mobility in the form of oxygen-bearing species (Tessalina et al., 2008; Yudovskaya et al., 2008).

Experimental data on the solubility of Os in oxidizing aqueous solutions under high temperature and pressure, are scarce and do not account for the possible contribution of oxidized Os-bearing species (e.g. OsO<sub>4(g)</sub>, Os<sub>2</sub>O<sub>3(g)</sub>). Theoretical estimations on Os mobility, however, suggest that under high temperature (523 °C) and oxidizing redox conditions (hematite – magnetite  $fO_2$ ) the fugacity of dissolved OsO<sub>4(g)</sub> in hydrothermal fluids could reach values of 10 ppt (Wood, 1987). Indirect evidence of OsO<sub>4(g)</sub> and Os<sub>2</sub>O<sub>3(g)</sub> formation has also been provided in experimental studies of OsO<sub>2</sub> thermal decomposition and calorimetry (Nikol'skii et al., 1967; O'Neill and Nell, 1997). Along with Os, experimental data have supported the possible oxidation of Ir at temperatures exceeding 700 °C (Peterson, 1976; O'Neill and Nell, 1997).

Here, I present a series of hydrothermal diamond anvil cell experiments conducted at temperatures ranging from 500 °C to 1000 °C and pressures resembling upper mantle/lower crust environments (<1500 MPa) to describe the role of saline solutions on the mobility of Os and Ir under oxidizing redox conditions. To evaluate the effect of pH and chloride concentrations, dilute solutions of NaOH, HCl and NaCl were used. Raman vibrational spectroscopy was employed to describe the composition of reactant fluids in real time and at in situ high temperatures and pressures.

### 2. METHODS

All mineral phases were obtained from Alfa Aesar and Speciality Products as high purity (99.996%; Os, MnO, Mn<sub>3</sub>O<sub>4</sub>) or metal basis grade powders and foils (99.7% OsCl<sub>3</sub>·H<sub>2</sub>O, 99.8% Ir, 99.99% MnO, 97% Mn<sub>3</sub>O<sub>4</sub>). Reactant aqueous solutions were prepared by making use of NaCl powders and NaOH pellets of 99.99% purity (Alfa Aesar). Ultrapure HCl acid was prepared by subboiling distillation at the Department of Terrestrial Magnetism, Carnegie Institution of Washington (CIW) (Kuehner et al., 1972; Walker, 1988; Shirey and Walker, 1995).

Experiments were performed by utilizing externally-heated hydrothermal diamond anvil cells (HDAC) (Bassett et al., 1996). The cell was equipped with low-fluorescence 1-mm culet ultrapure synthetic diamonds, and samples were contained in 125  $\mu m$  thick Ir gaskets (500  $\mu m$  diameter sample chamber). The diamonds were manufactured by chemical vapor deposition following CIW patented methodologies (Meng et al., 2012).

The diamond seat assembly was composed of a direct-sintered silicon carbide (UltraSIC, SC-30, Coorstek) that exhibits substantially greater hardness (26000 MPa) and thermal conductivity (150 W/m K) than the tungsten carbide. The SC-30 diamond seats allow HDAC experiments to be conducted to temperature of 1200 °C, and pressure of 3000 MPa with maximum operational temperatures of nearly 1600 °C¹ (Foustoukos and Mysen, 2015). Molybdenum wire was placed around the silicon carbide seats to heat the entire sample chamber. Temperature was moni-

tored with chromel–alumel thermocouples in contact with the upper and lower diamonds ( $\pm 1$  °C accuracy).

Raman vibrational data were collected with a JASCO NRS-3100 confocal microRaman spectrometer with an excitation laser line operating at 490.2 nm ( $\lambda_{ex}$ ) with maximum operating power of 37 mW imposed on the sample. Signal detection was accomplished through a Mitutoyo™ objective lens with a  $50 \times /0.42$  numerical aperture. The beam diameter was nearly 1 µm with a 10 µm focal depth. The acquired spectral windows were centered at 850 cm<sup>-1</sup> and 3400 cm<sup>-1</sup> with a frequency resolution of < 1 cm<sup>-1</sup> and  $\leq 2 \text{ cm}^{-1}$  at 2400 and 1200 grooves/mm, respectively. The signal was collected with a Peltier-cooled CCD at -69 °C (Andor™ Model DV401-F1 1024x128 pixel with 25 µm pixel size). The system was equipped with a holographic notch filter. All the Raman spectra collected were unpolarized. Acquisition time ranged from 5 to 120 s/ CCD window depending on signal intensity and volatility of the analyte. Two acquisitions per window were collected.

Pressure was determined at conditions by measuring the temperature/-pressure dependent Raman frequency shift of synthetic <sup>13</sup>C diamond (Schiferl et al., 1997). This method requires precise frequency measurements ( $\pm 0.1 \text{ cm}^{-1}$ ) of the fundamental band of <sup>13</sup>C. This was achieved by performing acquisitions at 2400 grooves/mm, and then normalizing the Raman shift to the Ne emission lines recorded on the same spectroscopic window (Bassett et al., 1996; Schiferl et al., 1997). The Ne emission lines at 540.06 nm ( $\lambda_{ex} = 490.2$  nm) were used as internal standard for the position of the spectrophotometer. The JASCO NRS-3100 is equipped with an internal Ne lamp. By adopting this methodology, the temperature/pressure dependent Raman frequency shift of the <sup>13</sup>C diamond was calibrated with an uncertainty of about  $\pm$  100 MPa at  $\pm$  40 MPa precision (Mysen and Yamashita, 2010). To further improve the accuracy of this method at low pressure conditions (<500 MPa), the pressure calibration experimental dataset was reevaluated to yield a pressure (P)/temperature (T) dependent function as follows:

$$P (MPa) = -165.73 + 262.01 \cdot (v_{P,T} - v_{0.1MPa,25^{\circ}C})$$

$$+ 2.488 \cdot T(^{\circ}C) + 0.008 \cdot T^{2}(^{\circ}C) - 3.22$$

$$* 10^{-6} \cdot T^{3}(^{\circ}C)$$
(1)

where  $v_{\rm P,T}$  and  $v_{0.1{\rm MPa},~25^{\circ}{\rm C}}$  are the <sup>13</sup>C diamond shifts at pressure and temperature (P, T) and at ambient conditions (0.1 MPa, 25 °C), respectively. The regression model has  $r^2 = 0.88$ , and a two-tail probability (*p*-value) of 0.000. The "lack of fit" test gives F-value of 0.28 and *p*-value of 0.989.

Curve-fitting of the Raman spectra was performed using the commercial software IGOR from Wavemetrics™. Background subtraction was conducted by fitting a third-order polynomial function through portions of the spectra with baseline signal intensity only (Long, 1977). Replicate measurements were acquired at the same beam spot and with the same instrumental parameters to minimize and constrain the uncertainties on spectra analysis and processing. The statistical treatment of experimental data was performed by utilizing XLisp-Stat in the technical graphic and data analysis software Arc 1.06 (http://www.stat.

http://www.coorstek.com/resource-library/library/8510-1364\_ceramic\_properties\_mp.pdf.

umn.edu/arc) (Cook and Weisberg, 1999). For the weight on least-squares fittings I applied the 1/(analytical error) <sup>2</sup> (York, 1969) and the error in fit parameters was derived from the covariance matrix as SQRT(cov<sub>ii</sub>), reflecting deviation of 2σ (95.4% confidence interval). The least-squares fittings were considered statistically significant if the two-tail probability (*p-value*) was of 0.05 or less (Devore, 1995; Cook and Weisberg, 1999; Press et al., 2007).

The thermodynamic properties of Ir, IrO<sub>2</sub>, IrO<sub>2(g)</sub>, Ir<sub>2</sub>O<sub>3</sub> (g), Os, OsO<sub>2</sub> and OsO<sub>4(g)</sub> are from the dataset of Knacke et al. (1991), and the experimental study of O'Neill and Nell (1997) (i.e. Table 3). The equilibrium constants for the Ir-IrO<sub>2(g)</sub> and Ir-IrO<sub>3(g)</sub> redox reactions were retrieved from Peterson (1976). Thermodynamic data for the Mnoxides and O<sub>2(g)</sub> are from Robie and Hemingway (1995). The standard state for liquid H<sub>2</sub>O is unit activity at the temperature/pressure conditions of this study (Aranovich and Newton, 1996; Foustoukos, 2016).

### 3. RESULTS

A total of 9 hydrothermal diamond anvil cell experiments were conducted (Table 1). Experiments were designed to study the effect of pH, dissolved chloride and redox conditions on the solubility and oxidation of Os and Ir under high temperatures (500-1000 °C) and pressures (29–1343 MPa). The composition of the reactant fluids ranged from highly acidic (0.5 N HCl, pH<sub>25°C</sub> = 1.0) to highly alkaline (0.5 N NaOH,  $pH_{25^{\circ}C} = 13.5$ ). Experiments were also conducted in the presence of a NaClenriched aqueous solution at similar levels of electrolyte concentrations (Cl<sup>-</sup>, Na<sup>+</sup>) and approximating those of seawater salinity (0.5 M NaCl). Oxygen fugacity ( $f_{O2}$ ) was constrained by the redox equilibria between MnO and Mn<sub>3</sub>O<sub>4</sub> at conditions more oxidizing than those expected under fayalite-magnetite-quartz equilibria ( $\pm 5 \Delta FMQ$ ) (Table 1). The attained redox conditions are more oxidizing than those proposed for the sub-arc mantle wedge (Parkinson and Arculus, 1999; Kelley and Cottrell, 2009). However, recent models advocated for progressive oxidation of mantle wedge by infiltrating subduction-derived fluids (Suzuki et al., 2011). Loaded samples were free of entrapped air bubbles.

Following established protocols (Mysen, 2015), phase equilibria amongst the reactant phases was initially approached from the highest temperature and pressure conditions at each experimental set. A reaction time of 3 h was allowed for each experimental condition. Times series measurements performed in situ at high temperatures and pressures indicate that equilibrium was reached at all conditions. Previous electrochemical studies involving MnO-Mn<sub>3</sub>O<sub>4</sub> equilibria employed reaction times ranging from 3 h to 5 min at temperatures ranging from 770 °C to 1390 °C (Huebner and Sato, 1970; Keller et al., 1991).

Raman spectra acquired in situ and in quenched samples revealed the presence of molecular H<sub>2</sub> (Table 2) identified by the Raman oscillation of H-H v<sub>1</sub> registered at  $\sim$ 4150 cm<sup>-1</sup> (Fig. 1) (Williams et al., 2002; Foustoukos and Mysen, 2012). Formation of hydrogen was observed in all the experiments as product of the metal/metal-oxide hydrothermal interaction. The concentrations of  $H_{2(aq)}$ expected for the MnO-Mn<sub>3</sub>O<sub>4</sub> redox equilibria at the suite of experimental conditions range within two orders of magnitude from  $\sim$ 1 to 500 mM. The averaged concentrations of  $H_{2(aq)}$  detected at in situ conditions (Table 2) are estimated to nearly 10 mM. The identification of trace amounts of H<sub>2</sub> (aq) was achieved by the employment of ultrapure CVD diamond anvils that reduce dramatically the background fluorescence levels in Raman spectra (Fig. 1b). These anvils were synthesized by microwave plasma assisted chemical vapor deposition under N<sub>2</sub>-free atmosphere (Meng et al., 2012). This technological advance resulted in low background levels across a wide frequency range, but most importantly, at the frequency regime that the oscillations of metal-oxygen bonds reside (e.g. Os=O, Mn-O) (300-1100 cm<sup>-1</sup>, Fig. 1a).

Control experiments were conducted by reacting pure  $\rm H_2O$  with Ir gaskets (experiments #7-#8, Table 1). Results revealed the formation of molecular  $\rm H_2$  at 700–800 °C and pressures of 543 MPa and 793 MPa, respectively (Table 2, Fig. 1b). The presence of H—H  $v_1$  was undetected at higher temperatures because of the enhanced blackbody radiation effects. Considering the  $\rm H_2$  detection limits approximated by the use of the same ultrapure CVD diamond anvils in the MnO-Mn<sub>3</sub>O<sub>4</sub> bearing experiments (#1–6), I hypothesize that the  $\rm H_{2(aq)}$  concentrations attained in the Ir-H<sub>2</sub>O exper-

Table 1
Description of the HDAC experiments conducted.

- total product of the transfer of the transfe							
#	Phase	T (°C)	P (MPa)	Redox	$\log^* f_{\text{O2}}$	ΔFMQ	Electrolyte
1	Os—Ir—H <sub>2</sub> O	500-800	240-452	MnO/Mn <sub>3</sub> O <sub>4</sub>	(-18.5) - (-9.7)	4.7–5.0	0.5 N NaOH
2	Ir—H <sub>2</sub> O	600-800	29-583	MnO/Mn <sub>3</sub> O <sub>4</sub>	(-15.1) - (-9.6)	4.6-4.8	0.5 N NaOH
3	$Os-Ir-H_2O^\#$	600-900	158-1343	$MnO/Mn_3O_4$	(-14.6) - (-8.1)	4.5-5.1	0.5 N HCl
4	Os-Ir-H <sub>2</sub> O	600-875	29-243	MnO/Mn <sub>3</sub> O <sub>4</sub>	(-15.1) - (-8.6)	4.8 - 5.0	0.5 N HCl
5	Ir—H <sub>2</sub> O	600-850	579-1013	$MnO/Mn_3O_4$	(-14.6) - (-8.4)	4.5-4.8	0.5 M NaCl
6	Os—Ir—H <sub>2</sub> O	600-900	343-1128	MnO/Mn <sub>3</sub> O <sub>4</sub>	(-14.8) - (-7.5)	4.6-4.9	0.5 M NaCl
7	Ir—H <sub>2</sub> O	500-900	317-1232	Natural diamond anvils			
8	Ir—H <sub>2</sub> O	500-1000	57-662	Ultrapure CVD diamond anvils			
9	0.5 M OsCl <sub>3</sub>	25-700	n.d.	0.5 N HCl			

<sup>\*</sup> Calculated based on the thermodynamic data of Robie and Hemingway (1995) and by assuming redox equilibrium at high temperatures and pressures. Estimated  $f_{O2}$  values are in excellent agreement with the experimental study of O'Neill and Pownceby (1993). Redox reaction:  $6\text{MnO} + \text{O}_{2 \text{ (g)}} = 2\text{Mn}_3\text{O}_4$ .

<sup>#</sup> Iridium gasket utilized was the one used in the experiment #2.

Table 2				
Volatile species	detected	in the	<b>HDAC</b>	experiments.

#	Phase	T (°C)	P (MPa)	Volatile
0.5 N NaOH				
1	Os—Ir	700, 800	438, 452	$\mathrm{H_2}^{\mathrm{a}}$
2	Ir	600, 700, 800	29, 254, 583	$H_2^{a}$
0.5 N HCl				_
3	Os—Ir	900	158	OsO <sub>4</sub> , H <sub>2</sub> <sup>a</sup>
4	Os—Ir	850, 875	150, 114	$OsO_4$
		600, 700, 800	28, 226, 243	$\mathrm{H}_2$
0.5 M NaCl				
6	Os—Ir	700, 800	543, 793	$\mathrm{H}_2$
Pure H <sub>2</sub> O				-
8	Ir	600, 700, 800	212, 411, 531	$\mathrm{H}_2$

<sup>&</sup>lt;sup>a</sup> Detected in the quenched gas phase.

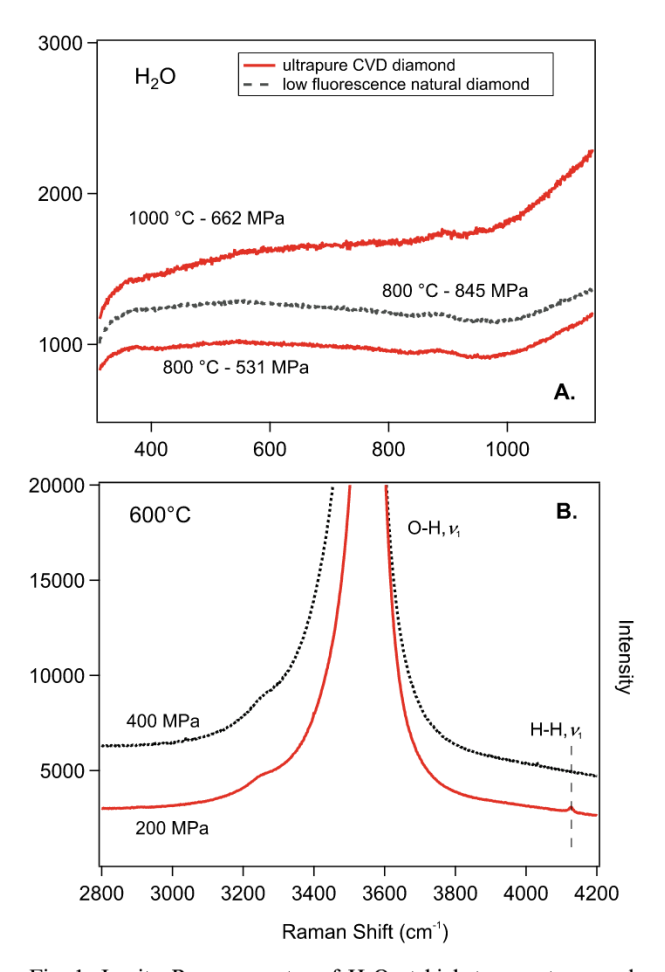


Fig. 1. In situ Raman spectra of  $H_2O$  at high temperatures and pressures by utilizing ultrapure CVD and natural diamond anvils (experiments #8, #9). The background fluorescence levels of the CVD diamonds are at least 50% lower than those recorded in high-quality low-fluorescence natural diamonds. (B) The use of the ultrapure CVD diamond anvils allowed the identification of H—H  $v_1$  associated with trace amounts of  $H_2$  possibly formed during hydrothermal oxidation of Ir gasket.

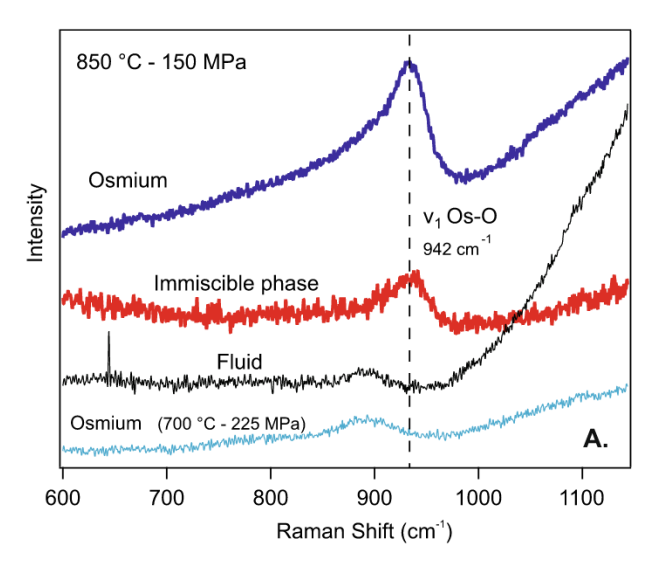
iments were lower than 1 mM. Trace amounts of  $H_{2(aq)}$ , thus, might correspond to the oxidation of either the Ir metal and/or any possible gasket impurities. Thermody-

namic data derived by previous studies on  $IrO_{2(s)}$  (Knacke et al., 1991; O'Neill and Nell, 1997), however, do not support precipitation of Ir-oxides at the experimental temperature and pressure conditions (Supplementary Fig. 1). Extremely low fugacities  $(10^{-15}-10^{-30})$  are also expected for the volatiles species  $IrO_{2(g)}$  and  $Ir_2O_{3(g)}$  (Peterson, 1976; Wood, 1987).

Furthermore, there is no evidence of a Ir-O bearing species on the Raman spectra acquired at high temperatures and pressures (Fig. 1a). Iridium oxide has been shown to exhibit three main Raman active modes at ~560 cm<sup>-1</sup>  $(E_g)$ ,  $\sim 730 \text{ cm}^{-1} (B_{2g}) \text{ and } \sim 750 \text{ cm}^{-1} (A_{1g})$  (Liao et al., 1997; Music et al., 2003; Korotcov et al., 2006). These vibrations were not present at high temperatures and pressures (Fig. 1b) and/or at the surface of the Ir gasket recovered after quenching. Even though H<sub>2</sub> formation is closely associated with the interaction of Ir gaskets with H2O at high temperatures and pressures, the possible role of contaminants in metal composition cannot be excluded. Nevertheless, to account for the possible contribution of Ir oxidation on H<sub>2</sub> formation, Os-bearing experiment #3 was conducted by utilizing a hydrothermally treated Ir gasket (experiment #2).

In the case of Os-bearing experiments, low pressure/high temperature conditions (<150 MPa, >850 °C) resulted in the exsolution of an immiscible phase in the matrix of the fluid phase (Fig. 2b). Raman spectra acquired from the immiscible bubbles indicate the presence of an Os=O bearing species exhibiting an asymmetric band at 936 cm<sup>-1</sup> (Fig. 2a). This frequency is consistent with the stretching vibration of Os=O  $v_1$  known for OsO<sub>4(g)</sub> (Levin, 1969; Louviot et al., 2013). Similar spectra were collected from the coexisting Os metal suggesting the possible formation of a Os-oxide on mineral surface. However, this Os=O bearing aqueous species was not detected in the fluid (Fig. 2a). Thus, it appears that vapor-fluid immiscibility resulted from phase separation and exsolution of Osenriched volatile species from the homogeneous fluid phase.

Acknowledging the role of acidic Cl-enriched fluids on Os solubility in the form of Os-Cl aqueous species (Wood, 1987; Xiong and Wood, 2000), a control experiment was conducted to investigate the frequency signature and distribution of the Os-Cl oscillations at high temperatures and pressures (experiment #9). The reactant fluid was a 0.5 M



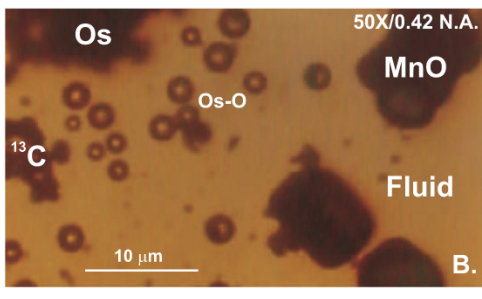


Fig. 2. Representative vibrational spectra (A) and microphotography (B) of phases present in high temperature/low pressure Os-Ir-MnO-Mn<sub>3</sub>O<sub>4</sub>-HCl experiments. The Raman spectrum of the immiscible bubbles exsolving from the fluid phase is indicative of a Os=O vibration supporting the presence of Os-O-bearing volatile species. Similarly, Os-oxides seem to emerge on the surface of Os metal. The Raman spectrum of Os metal at 700 °C, 225 MPa is shown for reference.

OsCl<sub>3</sub> – 0.5 N HCl aqueous solution. Raman data indicated a number of vibrational bands within the 300–1000 cm<sup>-1</sup> frequency region (Supplementary Fig. 2). The one located at 371 cm<sup>-1</sup> can be assigned to the fundamental vibrational band of Os—Cl according to Raman measurements in previous studies ( $v_1 \sim 395 \text{ cm}^{-1}$ ) (Levason et al., 1982; Volkov et al., 1996). Most interestingly, experimental data indicate the possible presence of an Os-related oscillation at 918 cm<sup>-1</sup>. Even through this band is in the proximity of the Os=O  $v_1$  discussed earlier (936 cm<sup>-1</sup> at 850 °C), it shifted to lower frequencies with temperature increase (898 cm<sup>-1</sup> at 200 °C). At higher temperatures (>200 °C), the vibrational features of the Os—Cl bonding environments became difficult to resolve from the background signal.

Raman spectra were also collected from the starting Mn-oxides. Results show a strong band corresponding to the stretching vibration of Mn—O (Supplementary Fig. 3). This vibron resides at 637 cm<sup>-1</sup> and 650 cm<sup>-1</sup> for the MnO and Mn<sub>3</sub>O, respectively. The frequency assignment of the Mn—O  $v_1$  in these oxides is in agreement with previous studies (Buciuman et al., 1999; Julien et al., 2004).

Therefore, taking into consideration the absence of any spectral interference across the 900–1000 cm<sup>-1</sup> for the dis-

solved species and mineral phases reacting at high temperature, the 936 cm<sup>-1</sup> oscillation observed in the Os-bearing experiments (Fig. 2) is attributed to Os=O bearing volatile species.

### 4. DISCUSSION

### 4.1. Hydrothermal oxidation of Os

Experimental and theoretical studies designed to constrain the extent and speciation of Os oxidation under hydrothermal conditions are very limited (Nikol'skii et al., 1967; O'Neill and Nell, 1997; Xiong and Wood, 2000). Osmium has been shown to be mobilized as chloro-complex (OsCl<sup>2-</sup>) when oxidized to the +2 state by reaction with Cl-enriched and acidic aqueous solutions (Xiong and Wood, 2000). These experiments were conducted at 500 °C and  $fO_2$  conditions similar to this study (Table 1). Earlier studies have also suggested the volatile transport of Os by Os-Cl complexation when reacting with molten NaCl at 1000 °C (Fleet and Wu, 1993; Fleet and Wu, 1995). For industrial applications, Os oxidation to Os(VIII) is associated with OsO<sub>4(g)</sub> synthesis (Livingstone, 1973).

Osmium tetroxide in solid form is highly volatile (b.p. 131 °C) and soluble in water (Livingstone, 1973). OsO<sub>4</sub> dissolves in aqueous fluids in the form of the weak perosmic acid (H<sub>2</sub>[OsO<sub>4</sub>(OH)<sub>2</sub>]). Sodium-bearing perosmate (Na<sub>3</sub>[-OsO<sub>4</sub>(OH)<sub>2</sub>]) has also been synthesized via the reaction of NaOH with Os metal under elevated  $fO_2$  (28 MPa) at 400 °C (Mogare et al., 2006). Hydrothermal transport of Os involving perosmate aqueous species has been suggested for the platinum-group element ore deposits in Florence Creek, Yukon (Barkov et al., 2008).

A series of thermodynamic calculations suggest that under redox conditions similar to this study ( $\Delta$ FMQ + 5), the concentration of OsO<sub>4(g)</sub> in hydrothermal fluids could range from 10 to 1 ppt at 523 °C and 923 °C, respectively (Wood, 1987). At 500 °C the concentration of OsCl<sup>2-</sup> dissolved in Cl-enriched aqueous solutions might reach 1700 ppb (Xiong and Wood, 2000). The aqueous complexation of Os with chloride, therefore, appears to be the dominant mechanism of metal transport in high  $fO_2$  supercritical aqueous fluids.

In the present experiments, oxidation of Os is inferred based on the Os=O  $v_1$  band identified by the in situ analysis of the immiscible phase exsolved from the homogeneous fluid phase (Fig. 2). Raman spectra didn't provide evidence of Os-Cl bearing species dissolved in either phase. Thermodynamic calculations indicate that formation of Os-oxides such as  $OsO_2$  and  $OsO_{4(g)}$  is inhibited (Fig. 3a). For example, under the oxidizing conditions attained  $(\Delta FMQ + 5)$ , the solubility of OsO<sub>4(g)</sub> is expected to reflect fugacities of less than 1 ppt (Wood, 1987). One has to consider, however, that experimental studies assessing phase equilibria in the Os-O2(g) system are very limited, and thus, the standard molar thermodynamic properties of Os oxides (OsO2, OsO3(g), OsO4(g)) extrapolated from high temperature conditions might not be accurate (Nikol'skii et al., 1967; O'Neill and Nell, 1997). Efforts were

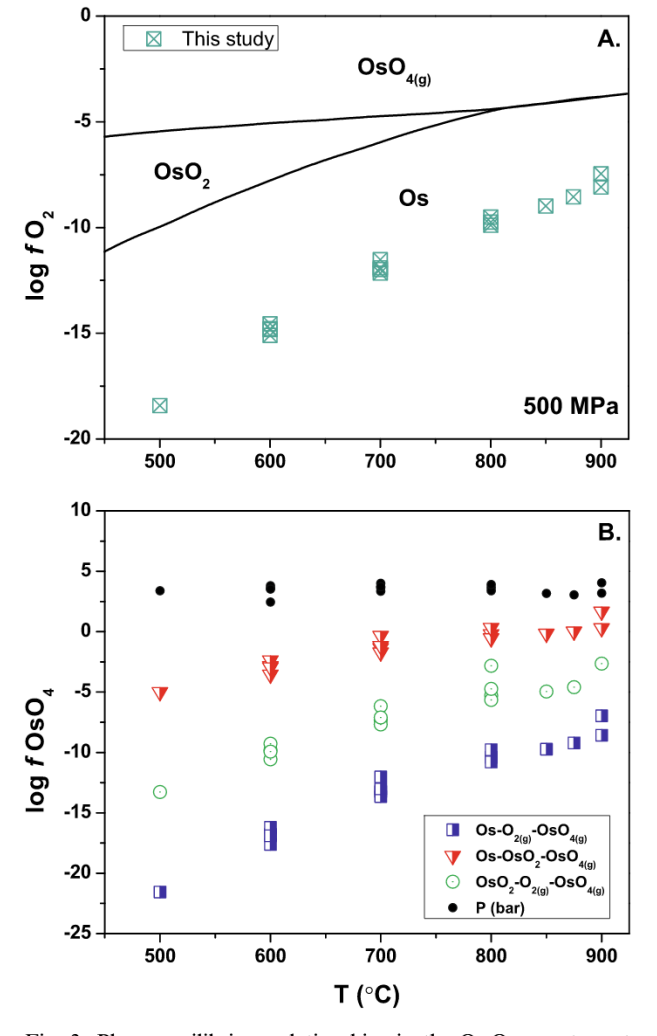


Fig. 3. Phase equilibrium relationships in the  $Os-O_{2(g)}$  system at 500 MPa and temperatures ranging from 500 to 900 °C. (A) The  $f_{O2}$  conditions estimated limit the thermodynamic drive required for metal oxidation. (B) Under these redox conditions, the equilibrium values of  $fOsO_4$  established between reactions within the  $Os-O_2$  system preclude formation of a discrete  $OsO_{4(g)}$ -bearing gas phase at elevated pressures.

made to reassess the thermodynamic properties of  $OsO_2$ ,  $OsO_{3(g)}$  and  $OsO_{4(g)}$  (Table 3) by comparing previous experimental data with the thermodynamic dataset of Knacke et al. (1991).

To the contrary, experimental evidence exist for oxidation of Os to  $OsO_2$  leading to the formation of  $OsO_{4(g)}$  and  $OsO_{3(g)}$  through disproportionation of the  $OsO_2$  at high temperatures. This was observed in the thermal decomposition experiments of Nikol'skii et al. (1967), as well as in the calorimetric measurements of O'Neill and Nell (1997). In both studies, the participation of  $OsO_{4(g)}$  and  $OsO_{3(g)}$  in equilibrium redox reactions was proposed to account for the  $fO_2$  attained at temperatures higher than  $800\,^{\circ}$ C. Therefore, considering that formation of  $OsO_{3(g)}$  requires more oxidizing conditions than  $OsO_{4(g)}$  (Nikol'skii et al., 1967), it is plausible that the latter represents the Os=O bearing species observed in the present experiments at 850– $950\,^{\circ}$ C (Fig. 2, Table 2).

For the exsolution of OsO<sub>4</sub> and the development of a discreet gas phase (e.g. Fig. 2a), fOsO<sub>4</sub> should exceed the confined pressure at experimental conditions. Elevated OsO<sub>4</sub> concentrations, however, cannot be supported by the existing thermodynamic data (Fig. 3b). Thus, if I assume that OsO<sub>4(g)</sub> is the main component of the immiscible phase, then I need to reconsider either the thermodynamic data of the OsO<sub>4(g)</sub> and/or the estimated redox and pressure conditions (Table 1). Clearly, phase separation was developed under high temperature and low pressure conditions. It is also possible, therefore, that observed immiscibility corresponds to the formation of a vapor/low Cl<sup>-</sup> phase enriched in volatile/neutral species (e.g. OsO<sub>4</sub> (g), HCl(aq)) in a fashion similar to the phase separation observed in the NaCl-H2O system (Sourirajan and Kennedy, 1962; Foustoukos and Seyfried, 2007). In this case, I cannot exclude the hypothesis that this vapor phase could be also enriched in perosmate  $(OsO_4(OH_2)^{2-})$ , perosmic acid or OsOCl<sub>4</sub>. However, very little is known about the phase relationships of the HCl-H<sub>2</sub>O system at supercritical conditions and there is a complete lack of any thermodynamic data for these Os-bearing aqueous species to consider in speciation models.

Table 3
Standard molar thermodynamic properties, heat capacity power function coefficients<sup>a</sup> and equilibrium constants for Os and Ir metals and oxides.

Phase	Ir	$IrO_2$	Os	$OsO_2$	$OsO_{4(g)}$
$\Delta_{\rm f} G^{\rm o}$ (J/mol)	0	-192836	0	-239128	-290808
$\Delta_f H^o (J/mol)$	0	-249366	0	-294553	-334067
S <sup>o</sup> (J/molšK)	35.5	51.045	32.635	51.882	297.834
α (J/molšK)	22.878	61.881	23.573	69.956	85.981
$b (\times 10^3) (\text{J/mols} \text{K}^2)$	7.037	20.418	3.807	10.376	20.418
$c \times 10^{-6}$ (JsK/mol)	0	-1.096	0	-1.418	-1.598
$2 \text{OsO}_2 = \text{Os} + \text{OsO}_{4(g)}$ $^{\text{b}} \text{log}(K_{\text{eq}}) = -11.01 \cdot 1000/\text{T(K)} + 9.16 (720-820 ^{\circ}\text{C})$					
$OsO_2 = Os + 2OsO_{3(g)}$ $blog(K_{eq}) = -12.45 \cdot 1000/T(K) + 10.18 (720-820  ^{\circ}C)$					

Data from Knacke et al. (1991) unless otherwise stated.

<sup>&</sup>lt;sup>a</sup>  $\Delta C_p^o = \alpha + bT + cT^{-2}$ .

<sup>&</sup>lt;sup>b</sup> Nikol'skii et al. (1967).

#### 4.2. Implication for Os mobility in subarc environments

The apparent mobility of Os in the form of a volatile oxide species provide insights on the role of hydrothermal fluids in affecting the distribution of highly siderophile elements in metasomatized rocks along the sub-arc mantle wedge and in the subcontinental lithosphere. A number of studies have demonstrated that Os mobility through hydrothermal fluid circulation accompanies mantle metasomatism. Altered xenoliths often are either depleted (Brandon et al., 1996; Widom et al., 2003; Saha et al., 2005; Senda et al., 2007; Suzuki et al., 2011; Liu et al., 2018) or enriched in Os (McInnes et al., 1999; Kepezhinskas et al., 2002; Lee, 2002; Alard et al., 2011; Rielli et al., 2018) relative to primitive mantle concentrations. In most cases, however, it appears that Os isotopic compositions are more radiogenic than those of the depleted mantle supporting the possible influx of radiogenic-Os enriched metasomatic fluids (e.g. Brandon et al., 1996; Widom, 2011). The formation of such fluids has been linked to the increased mobility of Re and Os in oxidizing, acidic and Cl-enriched hydrothermal fluids (Wood, 1987; Xiong and Wood, 2000; Widom, 2011). Experimental data presented here demonstrate Os mobility in the form of volatile species (e.g. OsO<sub>4(g)</sub>) even for slabderived fluids not saline enough to support formation of Os chloro-complexes (Righter et al., 2002).

To better understand conditions of Os mobility in the rock record, I investigated the relative distribution of Os and Ir in altered xenoliths that exhibit clear evidence of fluid induced metasomatism (McInnes et al., 1999; Kepezhinskas et al., 2002; Lee, 2002; Alard et al., 2011) (Supplementary Table 1). The compiled dataset represents bulk rock elemental and isotopic analysis of samples that contain both Os and Ir. For example, the contribution of slab-derived hydrous fluids enriched in Os has been inferred to support the radiogenic Os composition of metasomatized Lilir xenoliths (McInnes et al., 1999). The metasomatism of Monferrier and Big Creek peridotites has been linked to the percolation of oxidizing fluids enriched in S and radiogenic Os (Alard et al., 2011, Lee, 2002). In all cases, Ir is considered immobile during fluid-induced metasomatism in part because of the extremely low solubility of Ir in supercritical fluids (Peterson, 1976; Wood, 1987).

I coupled the behavior of Os with Ir to trace the flux of Os through the metasomatic process. Indeed, this pair exhibits a strong conservative behavior in mantle xenoliths consistent with the elemental distribution observed in mantle and chondritic samples (Barnes et al., 1985; Barnes et al., 2015; Becker et al., 2006; Puchtel et al., 2004; Tagle and Berlin, 2008). For the range of Os and Ir concentrations estimated for primitive upper mantle (PUM), the Os/Ir ratio ranges from 0.96 to 1.35 (e.g. Barnes et al., 2015).

Previous studies have proposed the important effect of metasomatic processes in enriching the Os composition of altered peridotites relative to Ir (Kepezhinskas et al., 2002; Alard et al., 2011; Rielli et al., 2018). To further illustrate the interplay between Os and Ir, Os concentrations were normalized to Ir (Fig. 4a) by plotting the Os/Ir ratios against the Ir content of bulk-rock. Deviations of the Os/Ir ratios from

the upper mantle values indicate possible addition of fluid-mobilized Os. This is consistent within the suite of samples that have been identified to have imprinted conditions of hydrothermal alteration (Fig. 4a). Furthermore, the radiogenic <sup>187</sup>Os/<sup>188</sup>Os composition of these samples can be readily correlated with the elevated Os/Ir ratios (Fig. 4b).

McInnes et al. (1999) have attributed the source of radiogenic Os in the metazomatized Lilir harzburgite to the flux of slab fluids derived from the altered oceanic crust of the Pacific Plate (<sup>187</sup>Os/<sup>188</sup>Os = 2.117). The metasomatized sample in Big Creek (1026 V) has been associated with hydrothermal fluids or garnet websterite of high time-integrated Re/Os ratio being the metasomatic agents (Lee, 2002). However, the latter appears less plausible consider-

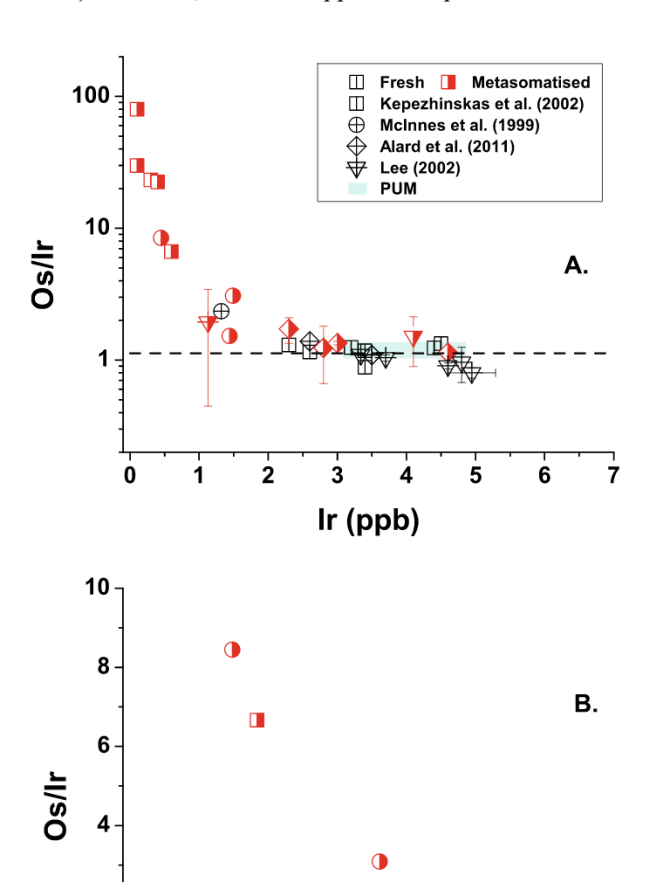


Fig. 4. Iridium-normalized concentrations of Os in metasomatized xenoliths along with the observed <sup>187</sup>Os/<sup>188</sup>Os bulk-rock compositions (Supplementary Table 1). (A) Fluid-induced metasomatic processes appear to be associated with Os enrichment relative to primitive upper mantle abundances. (B) Elevated Os/Ir ratios coupled with high <sup>187</sup>Os/<sup>188</sup>Os suggest that labile Os species may bear radiogenic signatures. The metasomatized harzburgites from Kamchacka (Bakening, 48-) that exhibit Os/Ir ratios > 22.5 (A; Supplementary Table 1) are characterized by <sup>187</sup>Os/<sup>188</sup>Os ratios ranging from 0.1352 to 0.1566 (Widom et al.., 2003).

<sup>187</sup>Os/<sup>188</sup>Os

0.15

0.20

0.25

2

0.10

ing that extremely elevated garnet websterite/peridotite mass ratios (250:1) are required to account for the abundance of metasomatic Os in 1026 V (Lee, 2002). For the Monferrier peridotites, subduction-related fluids derived from interaction with carbonatite melts have been suggested as the source of the radiogenic Os metasomatic agent (Alard et al., 2011). Carbonatites appear to exhibit elevated <sup>187</sup>Re/<sup>188</sup>Os and <sup>187</sup>Os/<sup>188</sup>Os ratios (Pearson et al., 1995; Blusztajn and Hegner, 2002; Escrig et al., 2005) with H<sub>2</sub>O-enriched carbonated melts shown to be enriched in dissolved ReO<sub>2</sub> (Foustoukos and Mysen, 2015). Similarly, carbonatite melt - slab fluid interactions have been proposed as the source of the radiogenic Os agent that metasomatized the Kamchatka mantle xenoliths (Widom et al., 2003). Interestingly enough, the conditions at which the Os = O bearing volatile species were observed (Fig. 2) are within the range of temperatures and pressures for hydrous melting of carbonate phases to occur (CaCO<sub>3</sub>-CaO-H<sub>2</sub>O) (Foustoukos and Mysen, 2015).

It is suggested, therefore, that the circulation of slabderived fluids in the sub-arc mantle could be deciphered by exploring the relative distribution of Os and Ir along with the Os isotope systematics. My experimental results indicate that in the presence of high temperature aqueous fluids at elevated pressure conditions, oxidation of Os could result in the formation of volatile Os-oxide aqueous species along with Cl-bearing aqueous complexes. These experimental data provide supporting evidence for the transport of oxygenbearing volatile species invoked to explain the elevated volatility of Os observed in volcanic fumaroles (Tessalina et al., 2008; Yudovskaya et al., 2008). It has been proposed that the continuous infiltration of slab fluids into the mantle wedge will lead to progressive oxidation and mobility of slabderived radiogenic Os component (Suzuki et al., 2011). Circulation of Os-enriched fluids in sub-arc could result in the precipitation of Os-bearing metal and/or sulfide phases during early-stage alteration of mantle peridotites (e.g. Foustoukos et al., 2015). Although the contribution of hydrothermal processes to the observed heterogeneity of <sup>187</sup>Os/<sup>188</sup>Os isotopes of mantle products is currently unknown to, the experimental data presented here provide evidence for a viable role of hydrothermalism as a an agent of Os mobilization and Os-isotope heterogeneity.

### **ACKNOWLEDGMENTS**

This research was conducted with support from the NSF-EAR-1347970, NSF-EAR-1761388 and NSF-OCE-1538671. I am thankful to Bjorn O. Mysen, Yufei Meng and Joseph Lai for providing ultrapure CVD diamonds. Constructive comments were provided by Steven B. Shirey, Michael Bizimis, James Brenan and two anonymous reviewers. The paper was benefitted from the constructive editorial recommendations of the Associate Editor, Richard J. Walker.

### APPENDIX A. SUPPLEMENTARY MATERIAL

Supplementary data to this article can be found online at https://doi.org/10.1016/j.gca.2019.04.019.

#### REFERENCES

- Alard O., Lorand J. P., Reisberg L., Bodinier J. L., Dautria J. M. and O'Reilly S. Y. (2011) Volatile-rich metasomatism in Montferrier Xenoliths (Southern France): Implications for the abundances of chalcophile and highly siderophile elements in the subcontinental mantle. *Journal of Petrology* 52, 2009–2045.
- Aranovich L. Y. and Newton R. C. (1996) H<sub>2</sub>O activity in concentrated NaCl solutions at high pressures and temperatures measured by the brucite-periclase equilibrium. *Contributions to Mineralogy and Petrology* **125**(2–3), 200–212.
- Barnes S. J., Naldrett A. J. and Gorton M. P. (1985) The origin of the fractionation of platinum-group elements in terrestrial magmas. *Chemical Geology* **53**, 303–323.
- Barnes S. J., Mungall J. E. and Maier W. D. (2015) Platinum group elements in mantle melts and mantle samples. *Lithos* 232, 395– 417
- Barkov A. Y., Martin R. F., LeBarge W. and Fedortchouk Y. (2008) Grains of Pt-Fe alloy and inclusions in a Pt-Fe alloy from Florence Creek, Yukon, Canada: Evidence for mobility of Os in a Na-H<sub>2</sub>O-Cl-rich fluid. *Canadian Mineralogist* 46, 343– 360.
- Bassett, W. A., Wu, T. C., Chou, I. M., Haselton, H. T., Jr., Frantz, J., Mysen, B. O., Huang, W. L., Sharma, K., and Schiferl, D., 1996. The hydrothermal diamond anvil cell (HDAC) and its applications. In: Dyar, M. D., McCammon C., and Schaefe, W. M. Eds.), Mineral Spectroscopy: A Tribute to Roger G. Burns. The Geochemical Society Special Publication, No. 5, p. 261-272.
- Becker H., Horan M. F., Walker R. J., Gao S., Lorand J. P. and Rudnick R. L. (2006) Highly siderophile element composition of the Earth's primitive upper mantle: Constraints from new data on peridotite massifs and xenoliths. *Geochimica Et Cosmochimica Acta* 70, 4528–4550.
- Blusztajn J. and Hegner E. (2002) Osmium isotopic systematics of melilitites from the tertiary Central European Volcanic Province in SW Germany. *Chemical Geology* 189, 91–103.
- Brandon A. D., Creaser R. A., Shirey S. B. and Carlson R. W. (1996) Osmium recycling in subduction zones. *Science* **272**, 861–864.
- Buciuman F., Patcas F., Craciun R. and Zahn D. R. T. (1999) Vibrational spectroscopy of bulk and supported manganese oxides. *Physical Chemistry Chemical Physics* 1, 185–190.
- Carlson R. W. (2005) Application of the Pt-Re-Os isotopic systems to mantle geochemistry and geochronology. *Lithos* 82, 249–272.
- Cook D. R. and Weisberg S. (1999) Applied regression including computing and graphics. Wiley-Interscience.
- Devore J. L. (1995) *Probability and statistics for engineering and the sciences*. Duxbury Press.
- Escrig S., Doucelance R., Moreira M. and Allegre C. J. (2005) Os isotope systematics in Fogo Island: Evidence for lower continental crust fragments under the Cape Verde southern islands. *Chemical Geology* **219**, 93–113.
- Fleet M. E. and Wu T. W. (1993) Volatile transport of platinumgroup elements in sulfide-chloride assemblages at 1000 °C. *Geochimica Et Cosmochimica Acta* **57**, 3519–3531.
- Fleet M. E. and Wu T. W. (1995) Volatile transport of precious metals at 1000 °C speciation, fractionation, and effect of basemetal sulfide. *Geochimica Et Cosmochimica Acta* **59**, 487–495.
- Foustoukos D. I. and Mysen B. O. (2012) D/H isotopic fractionation in the H<sub>2</sub>-H<sub>2</sub>O system at supercritical water conditions: Composition and hydrogen bonding effects. *Geochimica et Cosmochimica Acta* **86**, 88–102.
- Foustoukos D. I. and Mysen B. (2015) The structure of watersaturated carbonate melts. *American Mineralogist* 100, 35-46.

- Foustoukos D., Bizimis M., Frisby C. and Shirey S. (2015) Redox controls on Ni-Fe-PGE mineralization and Re/Os fractionation during serpentinization of abyssal peridotite. *Geochimica Et Cosmochimica Acta* 150, 11–25.
- Foustoukos D. I. (2016) On the ionic strength and electrical conductivity of crustal brines. *Chemical Geology* **447**, 183–190.
- Foustoukos D. I. and Seyfried W. E. (2007) Fluid phase separation processes in submarine hydrothermal systems. *Reviews in Mineralogy and Geochemistry* **65**, 213–239.
- Frezzotti M. L. and Ferrando S. (2015) The chemical behavior of fluids released during deep subduction based on fluid inclusions. *American Mineralogist* 100, 352–377.
- Huebner J. S. and Sato M. (1970) The oxygen fugacity-temperature relationships of manganese oxide and nickel oxide buffers. *American Mineralogist* 55, 934–952.
- Julien C. M., Massot M. and Poinsignon C. (2004) Lattice vibrations of manganese oxides - Part 1. Periodic structures. Spectrochimica Acta A 60, 689–700.
- Keller M., Xue J. and Dieckemann R. (1991) Electrochemical investigation of the oxygen activity at the manganosite-hausmmanite equilibrium. *Journal of Electrochemical Society* 138, 3398–3401.
- Kelley K. A. and Cottrell E. (2009) Water and the oxidation state of subduction zone magmas. *Science* **325**, 605–607.
- Kepezhinskas P., Defant M. J. and Widom E. (2002) Abundance and distribution of PGE and Au in the island-arc mantle: implications for sub-arc metasomatism. *Lithos* **60**, 113–128.
- Keppler H. (2017) Fluids and trace element transport in subduction zones. *American Mineralogist* **102**, 5–20.
- Knacke O., Kubaschewski O. and Hesselmann K. (1991) Thermochemical properties of inorganic substances. Springer-Verlag, Berlin, Heidelberg.
- Korotcov A. V., Huang Y. S., Tsai D. S. and Tiong K. K. (2006) Raman scattering characterization of vertical aligned 1D IrO<sub>2</sub> nanocrystals grown on single crystal oxide substrates. *Solid State Communications* 137, 310–314.
- Kuehner E. C., Murphy T. J., Alvarez R. and Paulsen P. J. (1972) Production and analysis of special high-purity acids purified by sub-boiling distillation. *Analytical Chemistry* 44, 2050–2056.
- Lee C. T. A. (2002) Platinum-group element geochemistry of peridotite xenoliths from the Sierra Nevada and the Basin and Range, California. *Geochimica et Cosmochimica Acta* 66, 3987– 4005.
- Levason W., Ogden J. S., Rest A. J. and Turff J. W. (1982) Tetrachloro-oxo-osmium(VI) a new synthesis, and matrix-isolation infrared and ultraviolet visible studies. *Journal of the Chemical Society-Dalton Transactions*, 1877–1878.
- Levin I. W. (1969) Low-temperature Raman spectra of solid osmium tetroxide and ruthenium tetroxide. *Inorganic Chemistry* 8, 1018–1021.
- Liao P. C., Chen C. S., Ho W. S., Huang Y. S. and Tiong K. K. (1997) Characterization of IrO<sub>2</sub> thin films by Raman spectroscopy. *Thin Solid Films* 301, 7-11.
- Liu C. Z., Xu Y. and Wu F. Y. (2018) Limited recycling of crustal osmium in forearc mantle during slab dehydration. *Geology* 46, 239–242.
- Livingstone S. E. (1973) The chemistry of ruthenium, rhodium, palladium, osmium, iridium and platinum. Pergamon Press.
- Long D. A. (1977) Raman Spectroscopy. MgGraw-Hill, New York.
  Louviot M., Boudon V., Bermejo D., Martinez R. Z. and Manceron L. (2013) High-resolution stimulated Raman spectroscopy and analysis of the v<sub>1</sub> band of osmium tetroxide.
  Journal of Raman Spectroscopy 44, 63–69.
- McInnes B. I. A., McBride J. S., Evans N. J., Lambert D. D. and Andrew A. S. (1999) Osmium isotope constraints on ore metal recycling in subduction zones. *Science* **286**, 512–516.

- Meng Y. F., Yan C. S., Krasnicki S., Liang Q., Lai J., Shu H. Y., Yu T., Steele A., Mao H. K. and Hemley R. J. (2012) High optical quality multicarat single crystal diamond produced by chemical vapor deposition. *Physica Status Solidi A-Applications* and Materials Science 209, 101–104.
- Mogare K. M., Klein W. and Jansen M. (2006) Trisodium dihydroxotetraoxoosmate(VII), Na<sub>3</sub>[OsO<sub>4</sub>(OH)<sub>2</sub>]. *Acta Crystallographica E* **62**, 152–154.
- Music S., Popovic S., Maljkovic M., Skoko Z., Furic K. and Gajovic A. (2003) Thermochemical formation of IrO<sub>2</sub> and Ir. Materials Letters 57, 4509–4514.
- Mysen B. O. and Yamashita S. (2010) Speciation and solubility of reduced C-O-H fluids in coexisting fluids and silicate melts determined in situ to 1.45 GPa and 800 °C. Geochimica Et Cosmochimica Acta 74, 4577–4588.
- Mysen B. O. (2015) An in-situ experimental study of Zr4+ transport capacity of water-rich fluids in the temperature and pressure range of the deep crust and upper mantle. *Progress in Earth and Planetary Science* 2(1), 38. https://doi.org/10.1186/ s40645-015-0070-5.
- Nikol'skii A. B., Semenov G. A. and Veschnyakova E. V. (1967) The thermal decomposition of osmium dioxide. *Russian Journal of Inorganic Chemistry* 12, 571.
- O'Neill H. S. and Nell J. (1997) Gibbs free energies of formation of RuO<sub>2</sub>, IrO<sub>2</sub>, and OsO<sub>2</sub>: A high-temperature electrochemical and calorimetric study. *Geochimica Et Cosmochimica Acta* **61**, 5279–5293
- O'Neill H. S. and Pownceby M. I. (1993) Thermodynamic data from redox reactions at high temperatures. 2. The MnO-Mn<sub>3</sub>O<sub>4</sub> oxygen buffer, and implications for the thermodynamic properties of MnO and Mn<sub>3</sub>O<sub>4</sub>. *Contributions to Mineralogy and Petrology* **114**, 315–320.
- Parkinson I. J. and Arculus R. J. (1999) The redox state of subduction zones: insights from arc-peridotites. *Chemical Geology* 160, 409–423.
- Pearson D. G., Shirey S. B., Carlson R. W., Boyd F. R., Pokhilenko N. P. and Shimizu N. (1995) Re-Os, Sm-Nd, and Rb-Sr isotope evidence for thick Archean lithospheric mantle beneath the Siberian Craton modified by multistage metasomatism. *Geochimica Et Cosmochimica Acta* 59, 959–977.
- Peterson D. E. (1976) Thermodynamics and trasport of gaseous Iridium oxides in multi-hundred-watt thermoelectric generators. Los Alamos Scientific Lab, New Mexico, USA.
- Press W. H., Teukolsky S. A., Vetterling W. T. and Flannery B. P. (2007) Numerical recipes in C: The art of scientific computing. *Cambridge University Press*, 661–666.
- Puchtel I. S., Humayun M., Campbell A. J., Sproule R. A. and Lesher C. M. (2004) Platinum group element geochemistry of komatiites from the Alexo and Pyke Hill areas, Ontario, Canada. Geochimica Et Cosmochimica Acta 68, 1361–1383.
- Righter K., Chesley J. T. and Ruiz J. (2002) Genesis of primitive, arc-type basalt: Constraints from Re, Os and Cl on the depth of melting and role of fluids. *Geology* **30**, 619–622.
- Rielli A., Tomkins A. G., Nebel O., Raveggi M., Jeon H., Martin L. and Avila J. N. (2018) Sulfur isotope and PGE systematics of metasomatised mantle wedge. *Earth and Planetary Science Letters* 497, 181–192.
- Robie, R. A. and Hemingway, B. S., 1995. Thermodynamic properties of minerals and related substances at 298.15K and 1 bar (105 pascals) pressure and at higher temperatures. United States Geological Survey Bulletin 2131, 462.
- Saha A., Basu A. R., Jacobsen S. B., Poreda R. J., Yin Q. Z. and Yogodzinski G. M. (2005) Slab devolatilization and Os and Pb mobility in the mantle wedge of the Kamchatka arc. *Earth and Planetary Science Letters* 236, 182–194.

- Schiferl D., Nicol M., Zaug J. M., Sharma S. K., Cooney T. F., Wang S.-Y., Anthony T. R. and Fleischer J. F. (1997) The diamond <sup>13</sup>C/<sup>12</sup>C isotope Raman pressure sensor system for high temperature/pressure diamond-anvil cells with reactive samples. *Journal of Applied Physics* **82**, 3256–3265.
- Senda R., Tanaka T. and Suzuki K. (2007) OsNd, and Sr isotopic and chemical compositions of ultramafic xenoliths from Kurose, SW Japan: Implications for contribution of slabderived material to wedge mantle. *Lithos* 95, 229–242.
- Shirey S. B. and Walker R. J. (1995) Carius tube digestion for lowblank rhenium-osmium analysis. *Analytical Chemistry* 67, 2136–2141
- Sourirajan S. and Kennedy G. C. (1962) The system NaCl-H<sub>2</sub>O at elevated temperatures and pressures. *American Journal of Science* **260**, 115–242.
- Suzuki K., Senda R. and Shimizu K. (2011) Osmium behavior in a subduction system elucidated from chromian spinel in Bonin Island beach sands. *Geology* 39, 999–1002.
- Tagle R. and Berlin J. (2008) A database of chondrite analyses including platinum group elements, Ni Co, Au, and Cr: Implications for the identification of chondritic projectiles. *Meteoritics & Planetary Science* 43, 541–559.
- Tessalina S. G., Yudovskaya M. A., Chaplygin I. V., Birck J. L. and Capmas F. (2008) Sources of unique rhenium enrichment in fumaroles and sulphides at Kudryavy volcano. *Geochimica Et Cosmochimica Acta* 72, 889–909.
- Volkov S. V., Pekhnyo V. I., Fokina Z. A. and Rybakov V. B. (1996) Halogen chalcogenide complexes of osmium(IV). *Polyhedron* 15, 4145–4154.
- Walker R. J. (1988) Low-Blank Chemical separation of rhenium and osmium from gram quantities of silicate rock for measurement by resonance ionization mass-spectrometry. *Analytical Chemistry* 60, 1231–1234.
- Widom E. (2011) Recognizing recycled osmium. *Geology* **39**, 1087–1088

- Widom E., Kepezhinskas P. and Defant M. (2003) The nature of metasomatism in the sub-arc mantle wedge: evidence from Re-Os isotopes in Kamchatka peridotite xenoliths. *Chemical Geology* 196, 283–306.
- Williams K. A., Pradhan B. K., Eklund P. C., Kostov M. K. and Cole M. W. (2002) Raman spectroscopic investigation of H<sub>2</sub>, HD, and D<sub>2</sub> physisorption on ropes of single-walled, carbon nanotubes. *Physical Review Letters* 88, 165502–165511.
- Wood S. A. (1987) Thermodynamic calculations of the volatility of the platinum group elements (PGE) - the PGE content of fluids at magmatic temperatures. *Geochimica Et Cosmochimica Acta* 51, 3041–3050.
- Xiong Y. and Wood S. A. (2000) Experimental quantification of hydrothermal solubility of platinum-group elements with special reference to porphyry copper environments. *Mineralogy* and Petrology 68, 1–28.
- York D. (1969) Least squares fitting of a straight line with correlated errors. Earth and Planetary Science Letters 5, 320– 324.
- Yudovskaya M. A., Tessalina S., Distler V. V., Chaplygin I. V., Chugaev A. V. and Dikov Y. P. (2008) Behavior of highlysiderophile elements during magma degassing: A case study at the Kudryavy volcano. *Chemical Geology* 248, 318–341.

### **FURTHER READING**

Ding K. and Seyfried, Jr., W. E. (1992) Determination of Fe-Cl complexing in the low pressure supercritical region (NaCl fluid): Iron solubility constraints on pH of subseafloor hydrothermal fluids. *Geochimica Et Cosmochimica Acta* 56, 3681–3692.

Associate editor: Richard J. Walker